Acta Pharmaceutica Sinica B 2023;13(9):3728−3743

Chinese Pharmaceutical Association
Institute of Materia Medica, Chinese Academy of Medical Sciences

Acta Pharmaceutica Sinica B

www.elsevier.com/locate/apsb
www.sciencedirect.com

ORIGINAL ARTICLE

Hepatic retinaldehyde deficiency is involved in diabetes deterioration by enhancing PCK1- and G6PC-mediated gluconeogenesis

Hanyu Yang[a,b,†], Mengxiang Su[c,†], Ming Liu[b], Yun Sheng[b], Liang Zhu[b], Lu Yang[a,b], Ruijing Mu[a,b], Jianjun Zou[d,*], Xiaodong Liu[a,b,*], Li Liu[a,b,*]

[a]*State Key Laboratory of Natural Medicines, Key Laboratory of Drug Metabolism and Pharmacokinetics, China Pharmaceutical University, Nanjing 210009, China*
[b]*Department of Pharmacology, School of Pharmacy, China Pharmaceutical University, Nanjing 210009, China*
[c]*Department of Pharmaceutical Analysis, School of Pharmacy, China Pharmaceutical University, Nanjing 210009, China*
[d]*Department of Clinical Pharmacology, Nanjing First Hospital, Nanjing Medical University, Nanjing 210006, China*

Received 29 January 2023; received in revised form 14 March 2023; accepted 6 May 2023

KEY WORDS

Type 2 diabetes;
Retinaldehyde;
Retinaldehyde dehydrogenase 1;
Gluconeogenesis;
Retinoid X receptor;
Oleic acid;
Glucose-6-phosphatase;
Phosphoenolpyruvate carboxykinase 1

Abstract Type 2 diabetes (T2D) is often accompanied with an induction of retinaldehyde dehydrogenase 1 (RALDH1 or ALDH1A1) expression and a consequent decrease in hepatic retinaldehyde (Rald) levels. However, the role of hepatic Rald deficiency in T2D progression remains unclear. In this study, we demonstrated that reversing T2D-mediated hepatic Rald deficiency by Rald or citral treatments, or liver-specific *Raldh1* silencing substantially lowered fasting glycemia levels, inhibited hepatic glucogenesis, and downregulated phosphoenolpyruvate carboxykinase 1 (PCK1) and glucose-6-phosphatase (G6PC) expression in diabetic *db/db* mice. Fasting glycemia and *Pck1/G6pc* mRNA expression levels were strongly negatively correlated with hepatic Rald levels, indicating the involvement of hepatic Rald depletion in T2D deterioration. A similar result that liver-specific *Raldh1* silencing improved glucose metabolism was also observed in high-fat diet-fed mice. In primary human hepatocytes and oleic acid-treated HepG2 cells, Rald or Rald + *RALDH1* silencing resulted in decreased glucose production and downregulated *PCK1*/*G6PC* mRNA and protein expression. Mechanistically, Rald downregulated direct repeat 1-mediated *PCK1* and *G6PC* expression by antagonizing retinoid X receptor α, as confirmed by

*Corresponding authors. Tel./fax: +86 25 83271060.
E-mail addresses: zoujianjun100@126.com (Jianjun Zou), xdliu@cpu.edu.cn (Xiaodong Liu), liulee@cpu.edu.cn (Li Liu).
[†]These authors made equal contributions to this work.
Peer review under the responsibility of Chinese Pharmaceutical Association and Institute of Materia Medica, Chinese Academy of Medical Sciences.

https://doi.org/10.1016/j.apsb.2023.06.014

luciferase reporter assays and molecular docking. These results highlight the link between hepatic Rald deficiency, glucose dyshomeostasis, and the progression of T2D, whilst also suggesting RALDH1 as a potential therapeutic target for T2D.

1. Introduction

Retinoids, including retinol, retinaldehyde (Rald), and retinoic acid (RA), are micronutrients essential for the maintenance of normal physiological processes[1]. The effects of retinoids on regulating glucose and lipid metabolism have also been demonstrated[2–4]. These functions of retinoids were considered to be mainly mediated by RA *via* the regulation of two major nuclear receptor families: retinoic acid receptors (RARs) and retinoid X receptors (RXRs)[4,5]. However, accumulating evidence has demonstrated that Rald, in addition to its role in visual regulation, also possesses several other important biological activities[6–8].

Retinoids are primarily stored in the liver, where approximately 80% of retinoids are stored in stellate cells, with the remainder being stored in parenchymal cells[9]. However, the large and abundant parenchymal cells account for over 70% of the enzymes and intracellular binding proteins involved in retinol metabolism[10,11]. In hepatocytes, retinol is oxidized to Rald by alcohol dehydrogenases or retinol dehydrogenases[12]. Rald is further irreversibly oxidized to RA by retinaldehyde dehydrogenases (RALDHs, also known as ALDH1As), which control the homeostasis of hepatic Rald[13].

Given this regulation mechanism, alcohol dehydrogenase 1 silenced mice have significantly lower levels of Rald[14]. Consequently, retinol dehydrogenase 1-null mice[12] and retinol dehydrogenase 10 knockout mice[15] have both been found to exhibit higher plasma exposure to glucose during glucose and insulin tolerance tests. In contrast, *Raldh1*$^{-/-}$ mice show increased Rald levels[14], alongside lower fasting blood glucose (FBG)[16] and lower plasma glucose during the glucose and insulin tolerance test[8]. We have previously reported that feeding a high-fat diet (HFD) significantly decreased the levels of Rald in the livers of rats, which was attributed to increases in the function and expression of hepatic RALDH1[17]. Furthermore, both RALDH1 inhibitors (such as citral and WIN 18,446) and Rald itself have been shown to improve glucose metabolism in *ob/ob* mice[8] and HFD-fed mice[18,19]. Based on these results, we deduced that hepatic Rald deficiency might contribute to hepatic glucose dyshomeostasis and the deterioration of T2D. To test this hypothesis, in the present study, we evaluated the influence of Rald, Rald + the RALDH1 inhibitor citral, or silencing of hepatic *Raldh1* in diabetic *db/db* mice *in vivo* and the impact of Rald on hepatic glucose metabolism in oleic acid (OA)-treated HepG2 cells and primary human hepatocytes as *in vitro* models.

The liver plays an essential role in systemic glucose homeostasis by regulating glucose uptake, utilization, gluconeogenesis, glycogenesis, and glycogenolysis, which are mainly controlled by enzymes such as glucokinase (GCK), phosphoenolpyruvate carboxykinase 1 (PCK1), and glucose-6-phosphatase (G6PC)[20,21]. Hepatic gluconeogenesis was reported to contribute to 75% of the hepatic glucose output in T2D[22]. Retinoids, especially RA, regulate the metabolism of hepatic glucose and lipids by affecting the RXR- and RAR-mediated expression of their target genes, such as *PCK1*, *G6PC*, *GCK*, and sterol regulatory element binding transcription factor 1 (*SREBF1*)[23]. In general, RXR must form homodimers or heterodimers with other nuclear receptors to regulate the transcription of their target genes[5] by binding response elements composed of two AGGTCA sites arranged in a direct repeat (DR) configuration with a characteristic inter-half-site spacing of 1−5 bp (known as DR1−DR5) of different genes[24]. The chemical structure of Rald is analogous to that of RA, indicating that Rald may also affect glucose metabolism by affecting retinoid receptors or by disturbing the affinity of retinoids to these receptors. Therefore, the final aim of this study was to investigate the associations between Rald, the *PCK1*/*G6PC* expression levels and the activation of these nuclear receptors. Collectively, these results highlight the link between hepatic Rald deficiency and hepatic glucose dyshomeostasis, thus providing a new mechanism for the progressive deterioration of T2D.

2. Materials and methods

2.1. Reagents

The retinoids were all-*trans* isomers unless otherwise indicated. All materials, antibodies, and primers used in this study are commercially available and are listed in Supporting Information Tables S1, S2, and S3, respectively.

2.2. Animals

Six-week-old male *db/db* mice (approximately 35 g), *db/m* mice (approximately 20 g), and C57BL/6J mice (approximately 20 g) were purchased from CAVENS Lab Animal Ltd. (Changzhou, China) and maintained under controlled environmental conditions (temperature, 24 ± 2 °C; humidity, 50 ± 5%, 12 h light/dark cycle) with free access to water and food. The experimental protocols were performed according to the Guide for the Care and Use of Laboratory Animals (National Institutes of Health, USA). Animal experiments were approved by the China Pharmaceutical University Animal Ethics Committee (protocol code No. 2019-06-016).

2.3. Rald and Rald+citral treatment in db/db mice

Following 1-week acclimation, 18 db/db mice (8 weeks old), were randomly assigned to the diabetic control (DM) group, the diabetic group treated with Rald (DM-R), or the diabetic group treated with Rald+citral (DM-RC). Six age-matched *db/m* mice were used as normal controls (CON). Rald (25 mg/kg) and citral (50 mg/kg) were administered to the mice *via* intraperitoneal

injection once daily for five weeks. Mice in the DM and CON groups received injection of vehicle only. The doses of the tested drugs were obtained from a previous report[8].

Physiological parameters such as body weight and water and food consumption were recorded daily during the treatments. FBG levels after 6 h of fasting were measured using a glucometer (Accu-Check; Roche, Mannheim, Germany) once a week. The intraperitoneal insulin tolerance test, intraperitoneal pyruvate tolerance test (ipPTT), and intraperitoneal glucose tolerance test (ipGTT) were performed on Days 24, 28, and 33, respectively. On the designated day, the experimental mice, after fasting for 6 h, received insulin (0.75 IU/kg), sodium pyruvate (1 g/kg), or glucose (0.75 g/kg). The blood glucose levels at 0 (baseline), 15, 30, 60, and 120 min post-injection were measured using a glucometer.

On Day 35, 6 h after the last dose, experimental mice were sacrificed under a yellow-light environment following isoflurane anesthesia. Tissues and blood samples were then immediately collected to measure Rald concentrations, biochemical parameters, and the levels of target genes and proteins. The concentrations of free fatty acids[25], Rald and RA[17] were all determined using high-performance liquid chromatography. Biochemical parameters were measured using the corresponding kits (Table S1).

2.4. *Liver-specific Raldh1 silencing in db/db mice*

The *Raldh1* gene in the livers of *db/db* mice was silenced using adeno-associated virus serotype 9 (AAV9)-*Raldh1*-shRNA (Hanheng, Shanghai, China). For AAV9-*Raldh1*-shRNA construction, two sequences of short hairpin RNA for *Raldh1* were designed, and the silencing efficiencies were determined in primary mouse hepatocytes (Supporting Information Fig. S1A−S1D). Sequence 2 (GGGTTAACTGCTATATGAT), which showed higher silencing efficiency, was selected for cloning into the vector.

Twelve *db/db* mice were randomly assigned to two groups, DM-ShCON mice and DM-ShRaldh1 mice, which were injected with the AAV9-Empty or AAV9-*Raldh1*-shRNA (2×10^{11} viral particles), respectively, *via* the tail vein. Body weight, water and food consumption, and FBG levels were monitored, as described above. Three weeks after transfection, *in vivo* imaging was performed using a Tanon ABL small animal imaging system (Tanon Science & Technology Co., Ltd., Shanghai, China) to confirm the specificity of virus infection. On Days 28 and 33 after transfection, the ipPTT and ipGTT were performed as described above. The experimental mice were sacrificed on Day 35 following transfection, with the corresponding parameters being measured as described above.

2.5. *HFD treatment to liver-specific Raldh1-silenced C57BL/6J mice*

Six-week-old male C57BL/6J mice ($n = 18$) were acclimated to the laboratory environment for 1 week. Twelve mice were injected with AAV9-Empty *via* the tail vein as control (ShCON) mice, whilst the six remaining mice were injected with AAV9-Raldh1-shRNA (2×10^{11} viral particles) to develop liver-specific *Raldh1*-silenced (ShRaldh1) mice. All mice were fed with a standard chow diet for 1 week, with six ShCON mice and six ShRaldh1 mice being switched to a HFD containing ~60% calories from fat (TP23300, TROPHIC Animal Feed High-Tech Co., Ltd., China) for 4 weeks to form the HFD-ShCON and HFD-shRaldh1 groups, respectively. The six remaining ShCON mice continued to be fed the standard chow diet to form the SCD-ShCON group. Details regarding the HFD feeding methods have been described in our previous report[17]. Food and water consumption, body weight, and FBG levels were monitored as described above. The ipPTT and ipGTT were performed 3 and 4 weeks after HFD initiation, respectively. On Day 37 following transfection, the experimental mice were sacrificed, with the corresponding parameters being measured as previously described.

2.6. *Cell culture and drug treatment*

HepG2 cells were purchased from the Chinese Academy of Medical Sciences (Shanghai, China) and cultured in Dulbecco's modified Eagle's medium containing 10% fetal bovine serum. To mimic the conditions of T2D, OA-treated HepG2 cells were established according to a previously described method[26,27]. In brief, once the cells reached approximately 40% confluence, they were cultured in medium containing 0.4 mmol/L OA for a further 72 h. Cellular levels of fatty acids and corresponding genes were then determined to confirm the successful development of the model. Subsequently, OA-treated HepG2 cells, with or without *RALDH1* silencing, were incubated in a culture medium containing Rald (2 μmol/L), or/and an agonist/antagonist of nuclear receptors [RXR, RAR, or peroxisome proliferator-activated receptor-gamma (PPARγ)] for 72 h, and the levels of glucose production, glucose utilization, and corresponding target gene and protein expression were measured.

Cryopreserved human hepatocytes (Cat. No. BQH1000.H15+) from four donors were purchased from Shanghai QuanYang Co., Ltd. (Shanghai, China). Following thawing, the hepatocytes were seeded in 48-well plates at a density of 1.5×10^5 cells/well. Twelve hours after seeding, the hepatocytes, with or without *RALDH1* silencing, were cultured in OptiCulture hepatocyte media (XenoTech, KS, USA) containing Rald (2 μmol/L) for another 72 h. The levels of glucose production and the expression of target genes and proteins were measured.

2.7. *RALDH1 knockdown with RNA interference*

Human primary hepatocytes and HepG2 cells were transfected with 100 nmol/L *RALDH1* small interfering RNA (siRALDH1) or scrambled negative control (siNC) (Gene-Pharma, Shanghai, China) and Lipofectamine 3000 (Invitrogen, CA, USA), according to the manufacturer's instructions. Twenty-four hours after transfection, the cells were subjected to the corresponding experiments described previously. The small interfering RNA sequence (5′-GGACAAUGCUGUUGAAUUUTT-3′) for human *RALDH1* was designed according to a previous report[28].

2.8. *Glucose production and utilization*

Glucose production and utilization assays were performed according to a previously described method[29]. Briefly, for glucose consumption, drug-treated cells were incubated with a fresh medium containing the tested agents and insulin (10 nmol/L) for 6 h. Glucose levels in the medium were then measured using a glucose assay kit (Jiancheng Bioengineering Institution, Nanjing, China). For glucose production assays, drug-treated cells were washed three times with phosphate-buffered saline and were incubated with glucose- and phenol red-free Dulbecco's modified Eagle's medium containing gluconeogenic substrates (20 mmol/L sodium lactate, 2 mmol/L sodium pyruvate, and 15 mmol/L HEPES) and the test agents for 3 h. Glucose formation in the medium was

determined by high-performance liquid chromatography, as previously reported[30].

2.9. Reverse transcription-quantitative polymerase chain reaction (qPCR)

Total mRNA was extracted from cells or tissues using RNAiso Plus Reagent (Takara, Japan) and reverse-transcribed into cDNA using HiScript III RT SuperMix for qPCR (Vazyme, Nanjing, China). The cDNA was then used as a template for qPCR amplification using qPCR SYBR Green Master Mix (Yeasen, Shanghai, China) and the corresponding primers (Table S3) on a LightCycler 96 real-time PCR system (Roche Applied Science, IN, USA) according to the manufacturer's instructions. Relative mRNA levels were normalized to *ACTB* using the comparative cycle threshold method.

2.10. Western blotting

Total protein was extracted from the liver and cells as previously described[29]. Proteins were separated using 8%−12% sodium dodecyl sulfate-polyacrylamide gel electrophoresis and transferred to a nitrocellulose membrane. After blocking for 2 h at room temperature with 5% nonfat dry milk, the blots were incubated overnight at 4 °C with the corresponding primary antibodies (Table S2). After washing with Tris-buffered saline with Tween, the blots were incubated with horseradish peroxidase-conjugated secondary antibodies for 1.5 h at room temperature. Protein levels were visualized using a highly-sensitive ECL Western Blotting substrate (Vazyme, Nanjing, China) and a gel imaging system (Tanon Science & Technology Co., Ltd., Shanghai, China).

2.11. Luciferase reporter assay

All plasmids were constructed by XinJia Medical Technology (Nanjing, China). The gene sequences for the ligand-binding domain (LBD) of RARα and RXRα were inserted into the pBIND plasmid to construct the pBIND-based Gal4-RARα LBD (RARα-LBD) and Gal4-RXRα LBD (RXRα-LBD) vectors. These plasmids, along with pGL4.35[luc2P/9XGAL4UAS/Hygro], were co-transfected into HEK293T cells for cell-based binding activity assays. pGL4.35-based luc2P-4XDR1 and luc2P-4XDR5, along with pBIND-based RXRα or RARα expression plasmids, were co-transfected into HEK293T cells for the transactivation assay of DR1-or DR5-triggered reporter gene expression.

HEK293T cells were seeded in 6-well plates for 12 h and then transfected with 2 μg of the above plasmids (Equimass) using Lipofectamine 3000 and P3000 according to the manufacturer's instructions. After 12 h of transfection, the cells were digested and divided into 96-well plates. Transfected cells were then incubated for an additional 12 h before treatment with the test agent. After 24 h of drug treatment, the cells were lysed and assayed for luciferase activity according to the instructions of the dual luciferase assay kit (Yeasen, Shanghai, China). The transfection efficiency was normalized to *Renilla* luciferase activity.

2.12. Molecular docking

The 3D crystal structure of RXRα (id:1FBY) was retrieved from the Protein Data Bank and prepared using Schrödinger Maestro 11.5. The ligand 3D structures were retrieved from the ZINC database and prepared using the Ligprep tool. Proteins and ligands were prepared using an OPLS3 force field. The scoring grid was defined based on the co-crystallized ligand (9-*cis*-RA) and then docked using the ligand docking tool. The grid box was the centroid of individual ligands, and the van der Waals scaling of receptors and ligands was 0.5. Other options were retained as the default parameters. After induced-fit docking, high-scoring induced-fit docking models were superimposed on the complex crystal structure to detect changes in the side chains.

2.13. Statistical analysis

Data were analyzed using GraphPad Prism version 8.0.2. A P value <0.05 indicates statistical significance. Unpaired two-tailed Student's t tests were used to compare two groups. One- or two-way analysis of variance, followed by Fisher's LSD multiple comparison tests, were used for comparisons among multiple groups.

3. Results

3.1. Hepatic Rald deficiency is involved in T2D deterioration

To confirm whether hepatic Rald deficiency contributes to the deterioration of T2D, *db/db* mice were treated with Rald (DM-R) or Rald+citral (DM-RC) for 5 weeks (Fig. 1A). The body weight change is shown in Fig. 1B. Rald or Rald+citral treatment substantially alleviated diabetic symptoms in *db/db* mice based on a decrease in food and water consumption and FBG levels (Fig. 1C−E, Supporting Information Table S4). Furthermore, Rald+citral showed potent therapeutic effects (Fig. 1C−E, Table S4). In diabetic control (DM) mice, FBG levels increased over time, from 17.0 ± 5.1 mmol/L at the beginning to 28.8 ± 3.2 mmol/L at the end of the five-week treatment, whereas FBG levels in DM-R mice only slightly increased, from 15.6 ± 3.7 mmol/L to 18.7 ± 6.7 mmol/L in the same period. In contrast, FBG levels in DM-RC mice decreased from 16.3 ± 6.0 mmol/L initially, to 13.9 ± 4.0 mmol/L after the treatment, although this difference was not statistically significant. Consequently, FBG levels in both DM-R and DM-RC mice at the end of the five-week treatment were significantly lower than those of DM mice (Fig. 1E and Table S4). Based on the ipPTT and ipGTT analysis results, compared with normal *db/m* (CON) mice, DM mice showed higher blood glucose exposure following sodium pyruvate or glucose loading, indicating an enhancement of gluconeogenesis and impairment of glucose utilization (Fig. 1F and G). Treatment with Rald or Rald+citral significantly decreased plasma glucose exposure following pyruvate or glucose administration in *db/db* mice (Fig. 1F and G). Insulin sensitivity tended to improve, although no significant difference was observed (Fig. 1H).

Compared with CON mice, DM mice showed significantly lower hepatic Rald concentrations (Fig. 1J), whereas diabetes tended to increase hepatic RA levels (Fig. 1K), which was in line with the upregulated expression of hepatic RALDH1 protein (Fig. 1I). Treatment with Rald or Rald+citral significantly increased hepatic Rald levels (Fig. 1J), but did not influence hepatic RA levels in *db/db* mice (Fig. 1K), which may be because the mRNA expression of cytochrome P450 family 26 subfamily A (*Cyp26a*), which encodes a RA metabolism enzyme, was sharply induced (Fig. 1L). Strong negative correlations of FBG levels

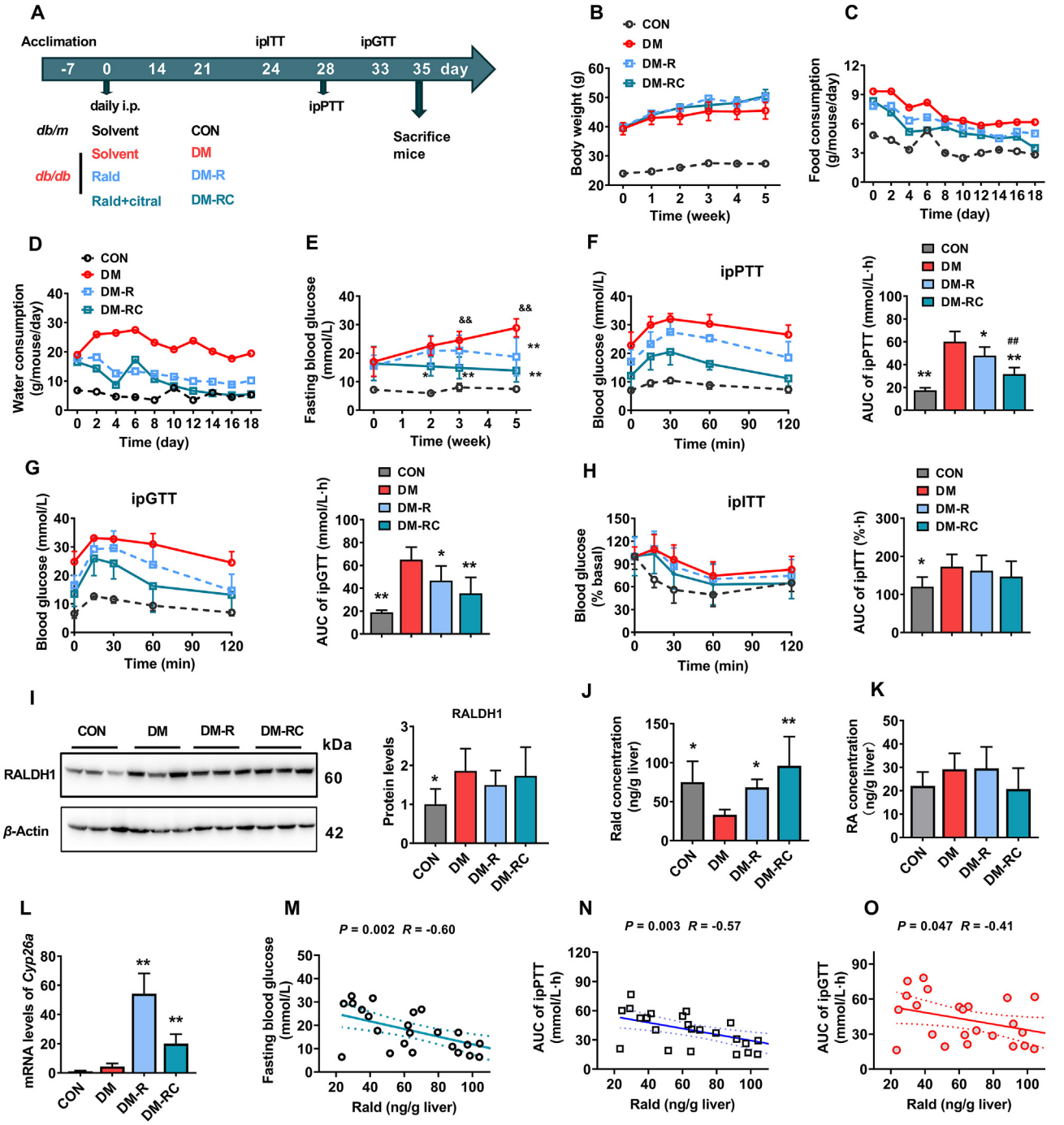

Figure 1 Effects of retinaldehyde (Rald) or Rald+citral treatment on type 2 diabetes (T2D) progression in *db/db* mice. Schematic diagram of the experiment (A). Changes in body weight (B), food intake (C), water consumption (D), and fasting blood glucose (FBG) levels (E) of *db/m* (CON) mice, *db/db* (DM) mice, Rald-treated *db/db* (DM-R) mice, and Rald+citral-treated *db/db* (DM-RC) mice. Blood glucose levels and their area under the curve (AUC) following intraperitoneal 1 g/kg sodium pyruvate (F), 0.75 g/kg glucose (G), or 1 IU/kg insulin (H) injection in CON, DM, DM-R, and DM-RC mice. The expression of RALDH1 protein (I), levels of Rald (J) and RA (K), and mRNA levels of *Cyp26a* (L) in the livers of CON, DM, DM-R, and DM-RC mice. Correlation analysis of hepatic Rald levels with FBG (M) and the AUC of the intraperitoneal pyruvate (N) or glucose tolerance test (O) in CON, DM, DM-R, and DM-RC mice. Data are mean ± SD, $n = 6$. $^{*}P < 0.05$, $^{**}P < 0.01$ *vs.* DM mice; $^{\#\#}P < 0.01$ *vs.* DM-R mice; $^{\&\&}P < 0.01$ *vs.* Week 0.

(Fig. 1M, $P = 0.002$) and the area under the curve (AUC) of the ipPTT (Fig. 1N, $P = 0.003$) and ipGTT (Fig. 1O, $P = 0.047$) with hepatic Rald concentrations were observed, which demonstrated that hepatic Rald deficiency is involved in the impairment of glucose metabolism in T2D.

3.2. *Liver-specific Raldh1 silencing improves hepatic glucose metabolism by increasing hepatic Rald levels in db/db mice*

In vivo imaging analysis showed that the livers of *db/db* mice were specifically infected with AAV9-*Raldh1*-shRNA to generate DM-

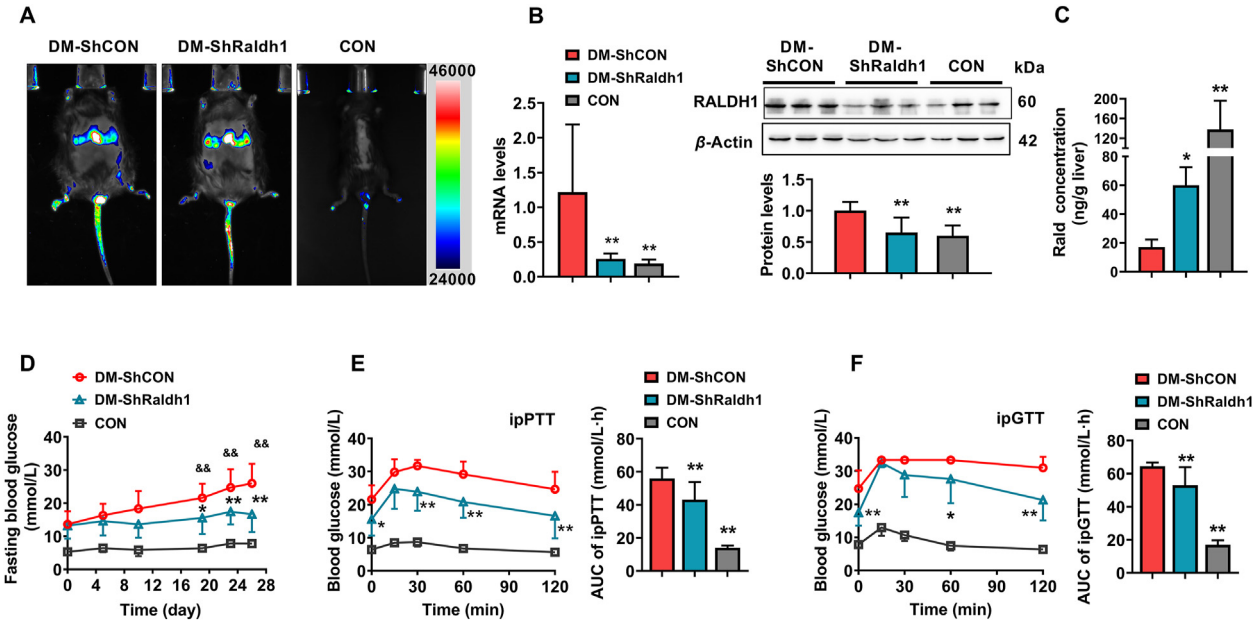

Figure 2 Liver-specific *Raldh1* silencing increases hepatic Rald levels to attenuate T2D deterioration. (A) *In vivo* imaging of CON mice (*db/m* mice receiving saline injection), DM-ShCON mice (*db/db* mice infected with AAV9-shEmpty), and DM-ShRaldh1 mice (*db/db* mice infected with AAV9-shRaldh1) at 3 weeks after AAV9 injection. Levels of hepatic RALDH1 mRNA and protein (B), hepatic Rald (C), and FBG (D) in CON, DM-ShCON, and DM-ShRaldh1 mice. Blood glucose levels and their AUC in each group of mice following intraperitoneal injection of 1 g/kg sodium pyruvate (E) or 0.75 g/kg glucose (F). Data are mean ± SD, $n = 6$. $^{*}P < 0.05$, $^{**}P < 0.01$ *vs.* DM-ShCON mice; $^{\&\&}P < 0.01$ *vs.* Day 0.

ShRaldh1 mice (Fig. 2A). Compared to DM-ShCON mice, DM-ShRaldh1 mice showed a significantly lower expression of hepatic RALDH1 at the protein and mRNA levels (Fig. 2B). Consequently, the hepatic Rald levels substantially increased from 17.1 ± 5.2 ng/g liver in DM-ShCON mice to 60.1 ± 12.5 ng/g liver in DM-ShRaldh1 mice (Fig. 2C).

Similar to the findings observed in Rald- and Rald+citral-treated *db/db* mice, liver-specific *Raldh1* silencing also improved diabetes symptoms in *db/db* mice (Fig. 2D−F and Supporting Information Table S5). DM-ShRaldh1 mice showed a similar body weight to that of DM-ShCON mice, although the consumption of food and water in DM-ShRaldh1 mice was lower than that in DM-ShCON mice (Fig. S1E−S1G). In contrast to DM-ShCON mice, FBG levels in DM-ShRaldh1 mice no longer increased over time (Fig. 2D). Significantly lower levels of blood glucose exposure during the ipPTT (Fig. 2E) and ipGTT (Fig. 2F) were also observed in the DM-ShRaldh1 mice.

3.3. *Decreases in hepatic Rald levels impair glucose metabolism by upregulating hepatic PCK1 and G6PC expression*

Compared with those of CON mice, DM mice showed significantly higher levels of PCK1 and G6PC proteins (Fig. 3A and B) and mRNA (Fig. 3C). The levels of GCK protein and mRNA also showed an increasing trend in DM mice, but this difference was not statistically significant. Treatment with Rald or Rald+citral substantially decreased the expression of PCK1 and G6PC at the protein and mRNA levels in the livers of *db/db* mice (Fig. 3A−C). The protein and mRNA expression levels of GCK were only significantly induced in the livers of DM-RC mice (Fig. 3A−C). Correlation analysis showed that hepatic Rald concentrations were negatively correlated with the mRNA levels of *Pck1* (Fig. 3D, $P = 0.0002$) and *G6pc* (Fig. 3E, $P = 0.013$) but not with those of *Gck* (Fig. 3F, $P = 0.90$), suggesting that hepatic Rald deficiency impairs hepatic glucose metabolism owing to upregulation of PCK1- and G6PC-mediated gluconeogenesis. The observation of a strong correlation between the AUC during the ipPTT and hepatic Rald concentration (Fig. 1N, $P = 0.003$) also supported the above deduction. These results were further confirmed by liver-specific *Raldh1* silencing, which significantly decreased the protein and mRNA expression levels of PCK1 and G6PC (Fig. 3G−I) in *db/db* mice, likely contributing to the observed increase in the levels of hepatic Rald (Fig. 2C). However, GCK protein levels were not significantly affected by liver-specific Raldh1 silencing (Fig. 3G−I).

3.4. *Liver-specific Raldh1 silencing attenuates the impairment of glucose metabolism in HFD-fed mice*

The role of hepatic Rald deficiency in the impairment of glucose metabolism was further observed in HFD-fed liver-specific *Raldh1*-silenced C57BL/6J (HFD-ShRaldh1) mice (Fig. 4A). HFD feeding significantly decreased hepatic Rald levels (Fig. 4B), whilst also increasing body weight (Fig. 4C), FBG levels (Fig. 4D), and serum glucose exposure after intraperitoneal administration of glucose or pyruvate in ShCON mice (Fig. 4F and G). Under the same HFD feeding conditions, ShRaldh1 mice had significantly higher liver Rald levels, as a result of the effective silencing of liver RALDH1 (Fig. 4B and Fig. S1H). Correspondingly, ShRaldh1 mice showed resistance to HFD-induced body weight gain (Fig. 4C) and the elevation of PCK1 and G6PC proteins (Fig. 4H) and FBG levels (Fig. 4D), without changing food consumption (Fig. 4E). The results of the ipGTT and ipPTT also demonstrated that ShRaldh1 mice showed reduced

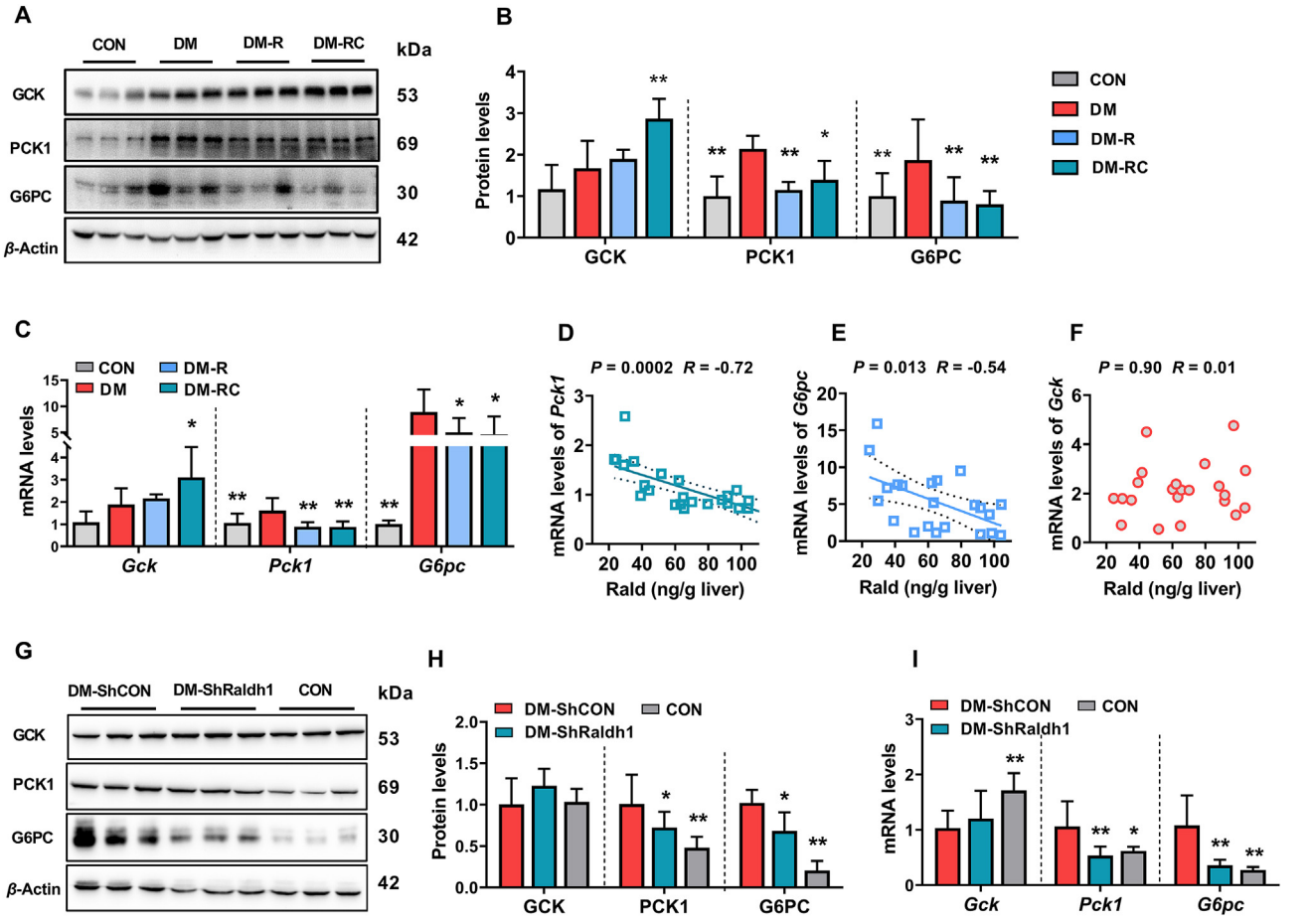

Figure 3 Decreases in hepatic Rald upregulates PCK1 and G6PC expression in *db/db* mice. GCK, PCK1, and G6PC protein levels (A, B) in the livers of CON, DM, DM-R, and DM-RC mice ($n = 6$). (C) *Gck*, *Pck1*, and *G6pc* mRNA levels in the livers of CON ($n = 5$), DM ($n = 6$), DM-R ($n = 6$), and DM-RC ($n = 6$) mice. Correlation analysis of hepatic Rald concentrations with the mRNA levels of *Pck1* (D), *G6pc* (E), and *Gck* (F). GCK, PCK1, and G6PC protein (G, H) and mRNA (I) levels in the livers of CON, DM-ShCON, and DM-ShRaldh1 mice ($n = 6$). Data are mean ± SD. $^*P < 0.05$, $^{**}P < 0.01$ *vs.* DM or DM-ShCON mice.

glucose exposure after glucose or pyruvate injections (Fig. 4F and G). Overall, these results suggest that the elevated levels of hepatic Rald improve glucose metabolism in HFD-fed mice.

3.5. Rald downregulates gluconeogenesis by inhibiting PCK1 and G6PC expression in OA-treated HepG2 cells and primary human hepatocytes

T2D is often associated with hepatic steatosis[31]. Therefore, OA-treated HepG2 cells were utilized to investigate the role of Rald in hepatic glucose metabolism. The OA-treated HepG2 cells were characterized by hepatic steatosis, as evidenced by the cellular accumulation of triglycerides (Fig. 5A), OA (Fig. 5B), and palmitic acid (Fig. 5C); impaired glucose utilization (Fig. 5D); and increased glucose production (Fig. 5E). OA-treated HepG2 cells also exhibited significantly higher mRNA levels of *G6PC* and *PCK1* than those of untreated control cells (Fig. 5F). OA treatment had no influence on RALDH1 activity and protein expression in HepG2 cells (Supporting Information Fig. S2A and S2B). Importantly, Rald decreased *PCK1* and *G6PC* mRNA expression in OA-treated HepG2 cells in a concentration-dependent manner (Fig. S2C and S2D). To prevent the transformation of Rald to RA, the expression of *RALDH1* in the OA-treated HepG2 cells was knocked down using small interfering RNA of *RALDH1* (siRALDH1) (Fig. S2E and S2F). Both Rald and Rald + SiRALDH1 significantly inhibited glucose production (Fig. 5G) and downregulated the expression of PCK1 mRNA (Fig. 5H) and protein (Fig. 5K). Rald + SiRALDH1 showed more potent inhibitory effects on PCK1 expression and significantly downregulated G6PC mRNA and protein expression (Fig. 5H and K). Rald and Rald + SiRALDH1 had little influence on glucose utilization (Fig. 5I) and the expression of GCK mRNA and protein (Fig. 5J and K).

The results observed in the OA-treated HepG2 cells were also replicated in human primary hepatocytes from four donors. The expression of *RALDH1* in human primary hepatocytes was also silenced (Fig. 5L) using SiRALDH1. Rald or Rald + siRALDH1 significantly decreased glucose production (Fig. 5M) and down-regulated the mRNA levels of *PCK1* and *G6PC* (Fig. 5N). In addition, significantly lower PCK1 and G6PC protein levels were also observed in human primary hepatocytes (from donors 2 and 3) that had been treated with Rald or Rald + SiRALDH1 (Fig. 5O).

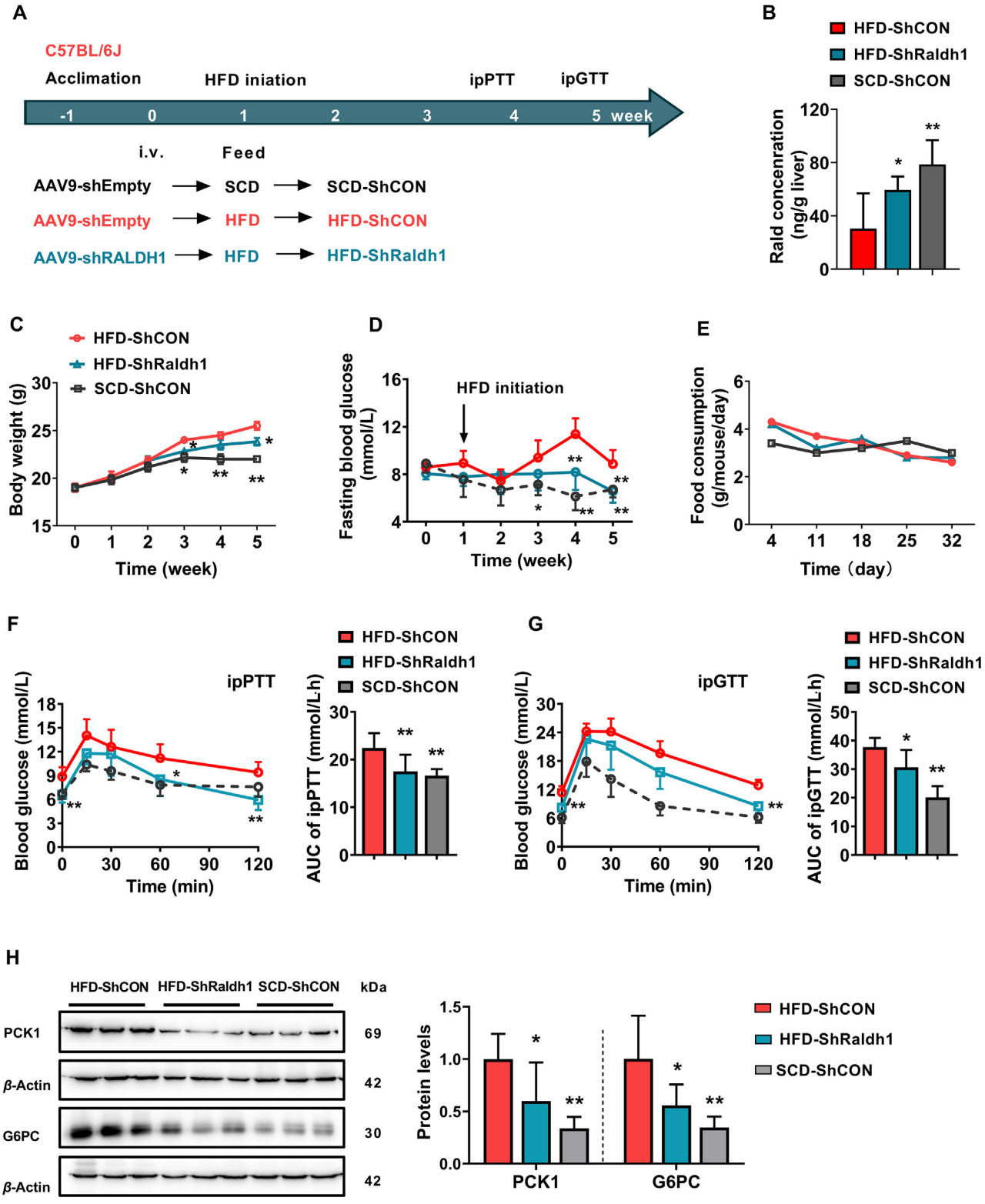

Figure 4 Liver-specific *Raldh1* silencing increases hepatic Rald to inhibit high-fat diet (HFD)-induced glucose dyshomeostasis. Schematic diagram of the experiment (A). Changes in the hepatic Rald levels (B), body weight (C), FBG levels (D), and food consumption (E) of SCD-ShCON mice (standard chow diet-fed AAV9-shEmpty-infected C57BL/6J mice), HFD-ShCON mice (HFD-fed AAV9-shEmpty-infected C57BL/6J mice), and HFD-ShRaldh1 mice (HFD-fed AAV9-shRaldh1-infected C57BL/6J mice). Blood glucose levels and their AUC in the SCD-ShCON, HFD-ShCON, and HFD-ShRaldh1 mice following intraperitoneal injection of 2 g/kg sodium pyruvate (F) or glucose (G). PCK1 and G6PC protein levels (H) in SCD-ShCON, HFD-ShCON, and HFD-ShRaldh1 mice. Data are mean ± SD, $n = 6$. $^{*}P < 0.05$, $^{**}P < 0.01$ *vs.* HFD-ShCON mice.

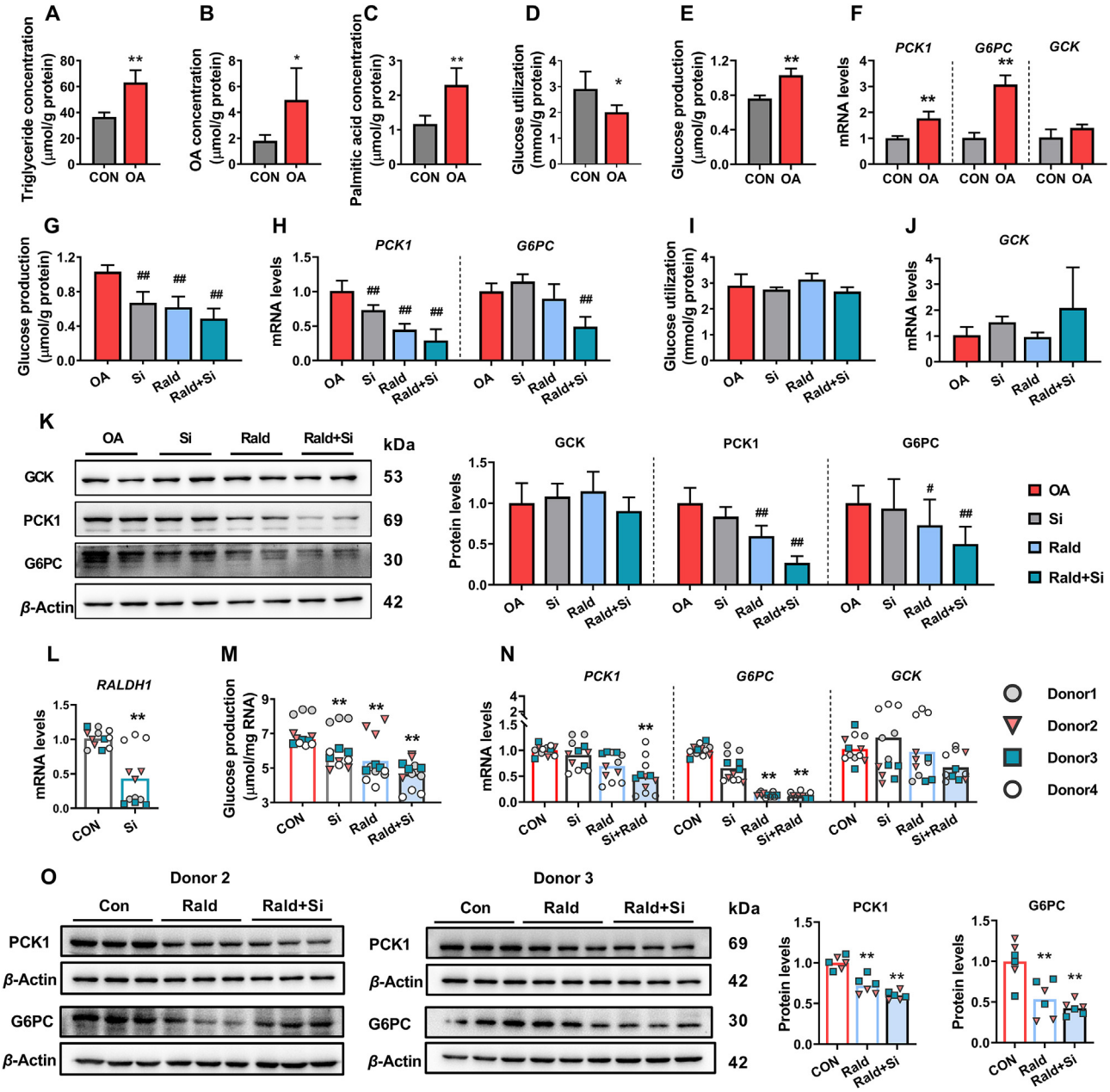

Figure 5 Effects of Rald and *RALDH1* silencing (Si) on the expression of enzymes related to glucose metabolism in oleic acid (OA)-treated HepG2 cells and primary human hepatocytes. Effects of OA treatment on the cellular levels of triglyceride (A), OA (B), palmitic acid (C), glucose utilization (D), glucose production (E), and mRNA levels of *PCK1*, *G6PC*, and *GCK* (F) ($n = 4$) in HepG2 cells. Effects of Rald, Si, and Rald + Si on glucose production (G), the mRNA expression of *PCK1* and *G6PC* (H), glucose utilization (I), and the mRNA expression of *GCK* (J) in OA-treated HepG2 cells ($n = 4$). Effects of Rald, Si, and Rald + Si on the expression of PCK1, G6PC, and GCK (K) proteins in OA-treated HepG2 cells ($n = 6$). Changes in the mRNA levels of *RALDH1* under Si treatment (L), changes in the levels of glucose production (M), and *PCK1*, *G6PC,* and *GCK* mRNA expression (N) under treatment with Si, Rald, or their combination in primary hepatocytes from four human donors ($n = 3$ for each donor). PCK1 and G6PC protein levels in primary hepatocytes from donors 2 and 3 ($n = 3$ for each donor) under Rald or Rald + Si treatment (O). Data are mean ± SD. $^{*}P < 0.05$, $^{**}P < 0.01$ *vs.* CON group; $^{\#}P < 0.05$, $^{\#\#}P < 0.01$ *vs.* OA group.

3.6. Rald suppresses PCK1 and G6PC expression by antagonizing RXR

In OA-treated HepG2 cells, Rald did not influence hepatocyte nuclear factor 4-alpha (HNF4α), peroxisome proliferator-activated receptor gamma coactivator 1 alpha (PGC1α), forkhead box O1 (FOXO1), and cAMP responsive element binding protein (CERB) protein expression or the phosphorylation levels of FOXO1 and CERB (Supporting Information Fig. S3), which excluded the involvement of these transcription factors known to participate in the regulation of *PCK1* and *G6PC* expression[32] in the Rald-mediated regulation of these genes.

The chemical structure of Rald is analogous to that of RA, suggesting that Rald may downregulate the expression of PCK1

and G6PC by affecting nuclear receptors. We found that both the RXR agonist LG100268 and the RAR agonist TTNPB induced *PCK1* expression in OA-treated HepG2 cells, which was significantly reversed by the RXR antagonist HX531 and RAR antagonist Ro 41−5253, respectively (Fig. 6A and B). LG100268 also significantly induced *G6PC* expression, whereas TTNPB only slightly increased the expression level of *G6PC*. The induction of *G6PC* expression was also attenuated by treatment with HX531 and Ro 41−5253 (Fig. 6A and B). Neither the PPARγ agonist rosiglitazone nor antagonist GW9662 affected the expression of *PCK1* and *G6PC* (Fig. 6C). These results overall indicate that RXR and RAR, but not PPARγ, might mediate *PCK1* and *G6PC* transcriptional regulation in OA-treated HepG2 cells.

RXRs can act as homodimers or obligatory heterodimerization partners for other nuclear receptors, including RAR. LG100268+TTNPB significantly upregulated the expression of *PCK1* and *G6PC* mRNA, which could be reversed by HX531 and Rald (Fig. 6D and E). The RAR antagonist Ro 41−5253 only inhibited *G6PC* expression induced by LG100268+TTNPB (Fig. 6E). Similar to the RXR antagonist HX531, Rald also reversed the upregulation of *PCK1* and *G6PC* expression induced by LG100268 but not by TTNPB (Fig. 6F−I). Both Rald and TTNPB significantly induced the expression of *CYP26A*, a known target gene of RAR[33], whilst Ro 41−5253 completely abolished the Rald-mediated induction of *CYP26A* (Fig. 6J). Moreover, Rald further enhanced the upregulation of *CYP26A* mRNA induced by LG100268+TTNPB, which was substantially reversed by Ro 41−5253 but not by HX531 (Fig. 6K). These results demonstrated that Rald is an agonist of RAR and an antagonist of RXR, thus indicating that Rald suppressed RXR-mediated *PCK1* and *G6PC* mRNA expression.

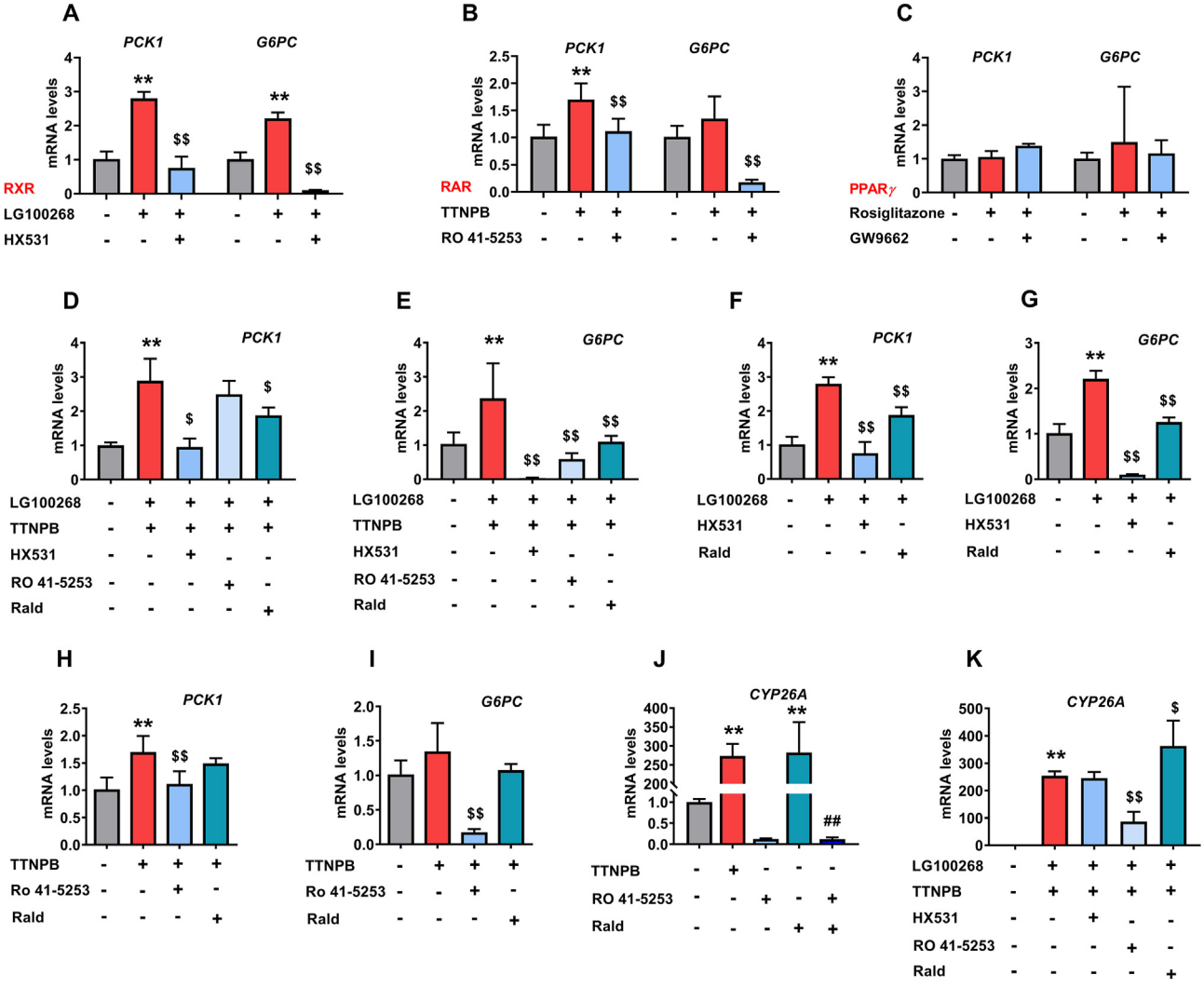

Figure 6 Rald inhibits *PCK1* and *G6PC* expression by antagonizing RXR. The effects of antagonists or agonists of RXR (HX531 or LG100268) (A), RAR (Ro 41−5253 or TTNPB) (B), and PPARγ (GW9662 or rosiglitazone) (C) on *PCK1* and *G6PC* mRNA expression in OA-treated HepG2 cells. The effects of HX531, Ro 41−5253, and Rald on LG100268+TTNPB-induced *PCK1* (D), *G6PC* (E), and *CYP26A* (K) mRNA expression. The effects of Rald on LG100268- (F and G) or TTNPB- (H and I) induced *PCK1* and *G6PC* mRNA expression. *CYP26A* gene expression under TTNPB, Ro 41−5253, and Rald treatment (J). In the above experiments, the concentrations of HX531, LG100268, TTNPB, GW9662, and rosiglitazone were 1 μmol/L; the concentration of Ro 41−5253 was 5 μmol/L; and the concentration of Rald was 2 μmol/L. Data are mean ± SD, $n = 4$. $^{**}P < 0.01$ *vs.* CON group; $^{\$}P < 0.05$, $^{\$\$}P < 0.01$ *vs.* LG100268, TTNPB, or LG100268+TTNPB group; $^{\#\#}P < 0.01$ *vs.* Rald group. RAR, retinoid acid receptor; RXR, retinoid X receptor; PPARγ, peroxisome proliferator-activated receptor-gamma.

3.7. *Rald antagonizes RXRα but activates RARα*

Luciferase reporter assays showed that Rald and RA stimulated RARα in a concentration-dependent manner, with EC_{50} values of 0.53 μmol/L and 16 nmol/L, respectively (Fig. 7A). Importantly, Rald antagonized RA-induced RARα activation (Fig. 7B and C), suggesting that Rald may act as a partial RARα agonist. RA, 9-*cis*-RA (9C-RA), and OA activated RXRα in a concentration-dependent manner, and the estimated EC_{50} values were 1.44 μmol/L, 47 nmol/L, and 58 μmol/L, respectively (Fig. 7D). Rald did not activate RXRα; in contrast, it significantly antagonized the RXRα activation mediated by RA (Fig. 7E and H) or OA (Fig. 7F and G). Furthermore, Rald inhibited OA-mediated RXRα activation in a concentration-dependent manner with an estimated IC_{50} of 0.18 μmol/L (Fig. 7G).

Molecular docking was performed to investigate the antagonistic effects of Rald on RXRα. The results show that Rald, RA, 9C-RA, and OA snugly fit into the RXRα ligand-binding pocket with different affinities (Rald > 9C-RA > RA > OA) (Fig. 7I and J). In contrast to 9C-RA, RA, and OA, Rald lacks a hydrogen bond with ALA-327, showing a unique molecular configuration in the LBD of RXRα (Fig. 7K). The RXRα structure is flexible upon binding different ligands and differs from RA, 9C-RA, and OA in that Rald abducts helix 11 in RXRα (Fig. 7K and L). The abduction of helices 11 and 12 inhibits conformational coactivator-binding surface formation in the LBD of nuclear receptors[34,35], which confirmed the antagonizing effect of Rald on RXRα.

3.8. *Rald downregulates the expression of PCK1 and G6PC by antagonizing RXR/DR1 activation*

RXR, as a homodimer or heterodimer with other nuclear receptors, plays an essential role in transcription regulation by binding different DR regions of genes[24]. In human primary hepatocytes, we found that Rald affected the expression of *SREBF1*, cytochrome P450 family 4 subfamily F member 2 (*CYP4F2*), and *RARB2*, which have been reported to be regulated by different DRs. *SREBF1* and *CYP4F2* are mainly regulated by DR1[36,37], whilst *GCK* and cellular retinoic acid binding protein 2 (*CRABP2*) are mainly regulated by DR2[38,39], and the expression of *RARB2* and *CYP26A* is primarily regulated by DR5[40,41]. Our results show that the regulatory model of Rald on *PCK1* and *G6PC* expression was more similar and correlated to that of *SREBF1* and *CYP4F2*, which are DR1-regulated genes ($P < 0.0001$) (Fig. 8A and Supporting Information Fig. S4).

The RAR:RXR heterodimer binds to both the DR1 and DR5 regions of genes, whereas the RXR:RXR homodimer binds only to the DR1 region[42]. To further confirm our findings, fluorescent expression plasmids containing the DR1 or DR5 motif and the full-length RXRα or RARα gene were simultaneously transfected into HEK293T cells to construct three luciferase reporter systems (RXR:RXR-DR1, RAR:RXR-DR1, and RAR:RXR-DR5); 9C-RA was used to activate the luciferase reporter system (Fig. 8B−D). These results show the different effects of Rald on the relative luciferase activity induced by 9C-RA. In the RXR:RXR-DR1 system, both Rald and the RXR antagonist HX531 decreased the relative luciferase activity induced by 9C-RA in a concentration-dependent manner (Fig. 8B). In the RAR:RXR-DR1 system, low-concentration Rald decreased, whereas high-concentration Rald (5 μmol/L) increased the relative luciferase activity induced by 9C-RA; however, HX531 only showed inhibitory effects (Fig. 8C). In the RAR:RXR-DR5 system, Rald enhanced the relative luciferase activity induced by 9C-RA (Fig. 8D). These results demonstrate that Rald inhibits RXR/DR1-mediated gene expression but increases RAR/DR5-mediated gene expression, which explains the observed inhibitory effect of Rald on *PCK1* and *G6PC* expression and the inducing effect of Rald on *CYP26A* expression.

4. Discussion

T2D is a progressive disease and chronically elevated FBG can worsen diabetes over time. Our findings demonstrate that increasing hepatic Rald levels through Rald or citral treatments or liver-specific *Raldh1* silencing, lowered FBG levels, improved glucose metabolism, and attenuated T2D deterioration in *db/db* mice. We also observed strong negative associations between hepatic Rald levels and FBG and blood glucose exposure during the ipPTT. These results demonstrate that hepatic Rald deficiency is involved in glucose dyshomeostasis and T2D deterioration. To our knowledge, this is the first report to reveal the contributions of hepatic Rald deficiency in the progression of T2D.

The liver is responsible for the disposal of approximately 60%−65% of the oral glucose load[43] and approximately 90% of endogenous glucose production[44]. Under T2D conditions, 75% of the hepatic glucose output is attributed to hepatic gluconeogenesis[22]. Increased hepatic glucose production contributes to hyperglycemia in T2D[45,46]. Our findings demonstrated that in *db/db* mice, Rald, Rald+citral, and liver-specific *Raldh1* silencing substantially reversed the induction of hepatic PCK1 and G6PC, which was in line with the lower FBG and plasma glucose levels observed during the ipPTT. PCK1 and G6PC are the key enzymes involved in hepatic gluconeogenesis. Therefore, these results indicate that a decrease in hepatic Rald levels drives a systemic change in hepatic glucose metabolism, particularly in the enhancement of glucogenesis *via* the induction of PCK1 and G6PC expression, thus elevating FBG levels, and aggravating T2D. The negative relationship between hepatic Rald concentrations and *Pck1* and *G6pc* mRNA expression also supports this deduction. Our previous study showed that HFD-induced obesity upregulated hepatic RALDH1 expression to decrease Rald levels[17]. The role of hepatic Rald deficiency in the impairment in glucose metabolism was further verified in HFD-fed mice. These findings were consistent with those in *db/db* mice that liver-specific *Raldh1* silencing elevated hepatic Rald levels to repress the HFD-induced elevation in hepatic gluconeogenesis and PCK1/G6PC expression. Similar results were observed in *Raldh1*$^{-/-}$ mice, with increased Rald levels[14], which also show significantly lower levels of hepatic glucose production and decreased PCK1 and G6PC protein and mRNA expression, independent of body mass and insulin sensitivity[16].

The role of Rald in the induction of PCK1 and G6PC expression was investigated using OA-treated HepG2 cells. Rald and Rald + siRALDH1 treatment inhibited glucose production and downregulated the mRNA and protein levels of PCK1 and G6PC, but had little effect on glucose utilization and the expression of GCK mRNA and protein. The results from OA-treated HepG2 cells were almost identical to those in primary hepatocytes from four human donors. Many transcription factors (such as HNF4α, PGC1α, FOXO1, and CERB) regulate *PCK1* and *G6PC* expression[32]; however, our study demonstrate that Rald did not influence the expression or activation of these transcription factors. RA exerts its biological effects mainly by activating RXR,

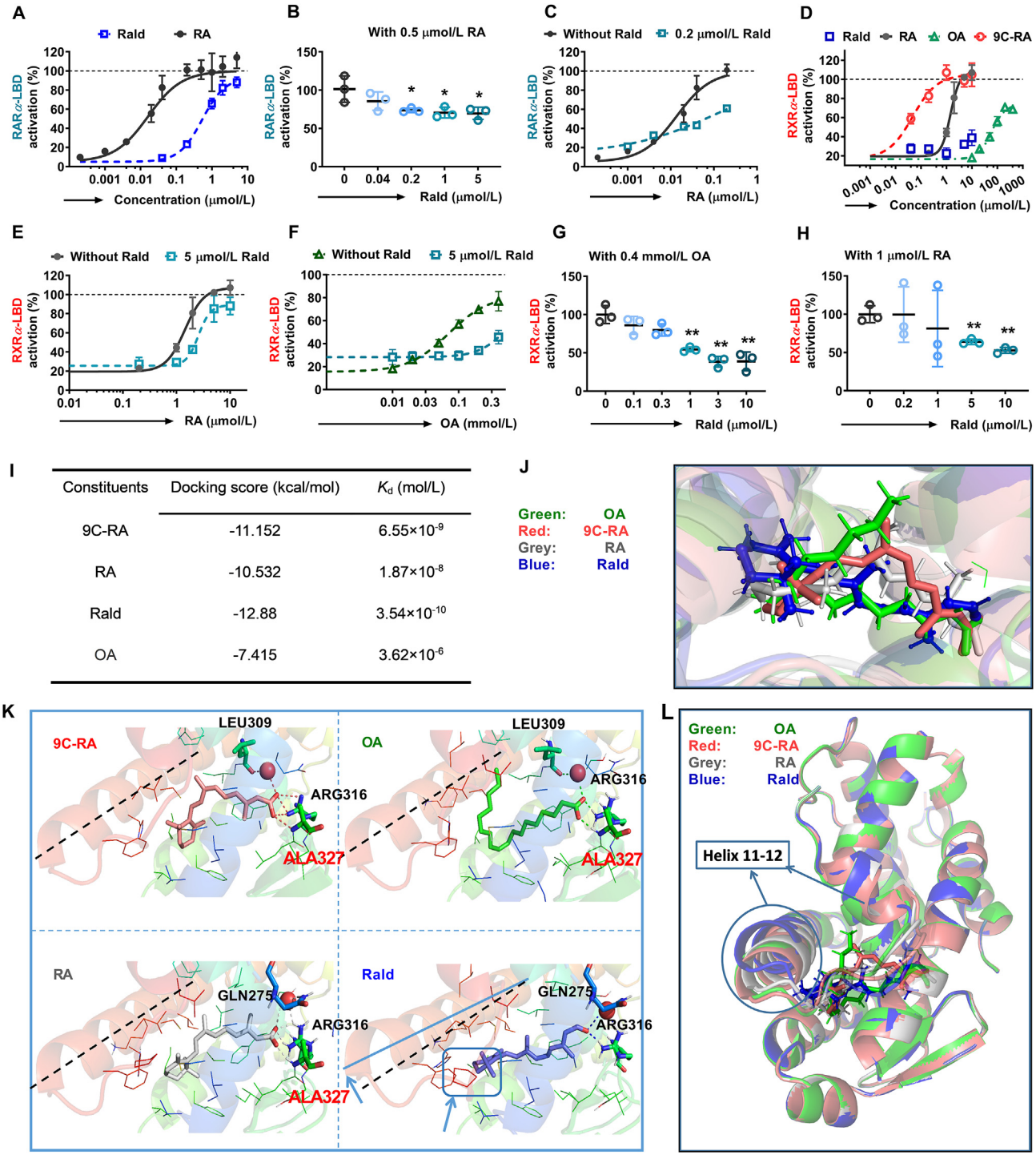

Figure 7 Effects of Rald on RXRα and RARα activation. The effects of Rald or RA on RARα-ligand-binding domain (LBD) activation (A). The effects of concentration-elevated Rald with 0.5 μmol/L RA (B) and concentration-elevated RA with or without 0.2 μmol/L Rald (C) on RARα-LBD activation. The effects of Rald, RA, OA, or 9-*cis*-RA (9C-RA) on RXRα-LBD activation (D). The effects of concentration-elevated RA (E) or OA (F) with or without 5 μmol/L Rald on RXRα-LBD activation. The effects of concentration-elevated Rald with 0.4 mmol/L OA (G) or 1 μmol/L RA (H) on RXRα-LBD activation. (I) The docking score of Rald, RA, OA, or 9C-RA calculated by the glide function of Schrödinger Maestro 11.5. Close-up view of the above ligands (J) and their binding modes (K) in the RXRα binding pocket. (L) Superimposition of the RXRα crystal structures with different ligands bound. Data are mean ± SD, $n = 3$. $^*P < 0.05$, $^{**}P < 0.01$ *vs.* concentration 0.

RAR, or PPARγ[47–49]. The chemical structure of Rald is analogous to that of RA, indicating that Rald may also regulate *PCK1* and *G6PC* mRNA levels by affecting these three receptors. Consistent with previous reports[16,50], we found that the activation of RAR and RXR induced *PCK1* and *G6PC* mRNA expression. Several reports have demonstrated that PPARγ is involved in the expression of *G6PC* and *PCK1* in adipose cells[51,52]. However, in line with the findings observed in HepG2 cells[53], the activation of

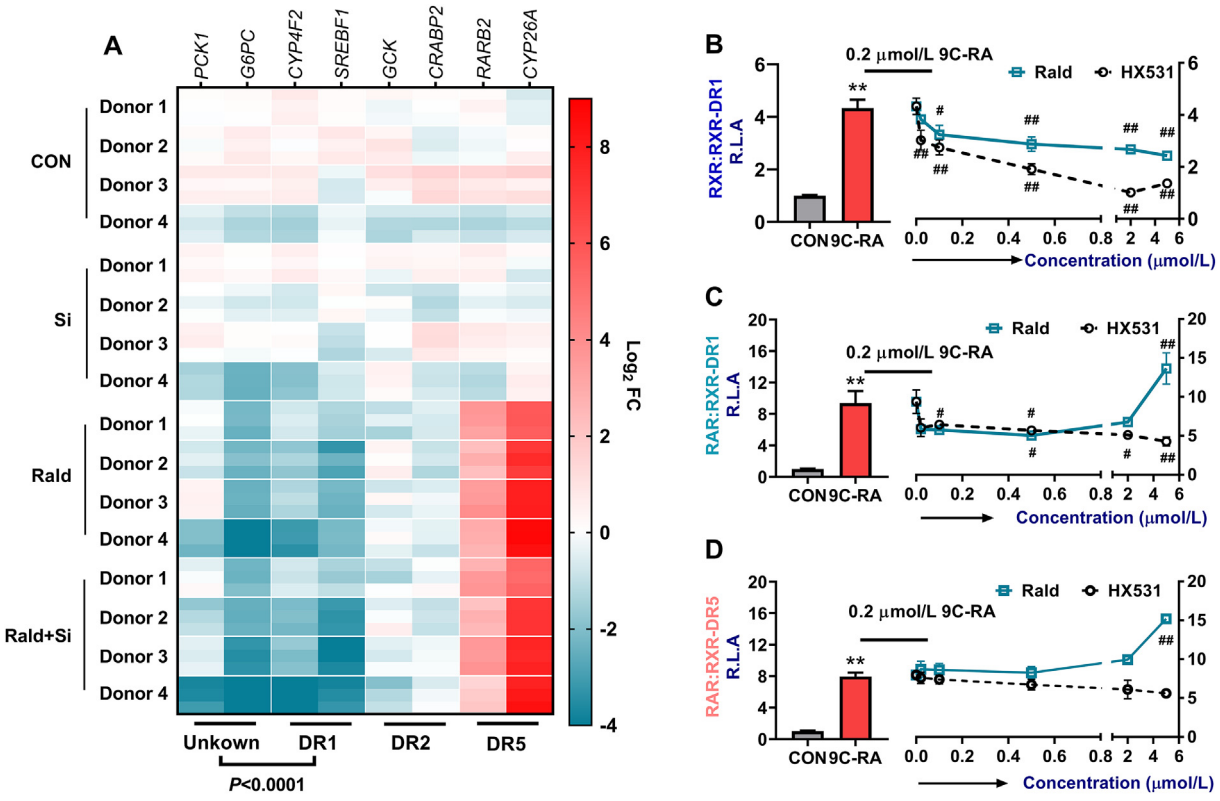

Figure 8 Rald downregulates *PCK1* and *G6PC* expression by inhibiting RXR/DR1 activation. (A) Heatmap showing the changes in the levels of different genes in human primary hepatocytes under Rald treatment, *RALDH1* silencing (Si), and combination of them ($n = 3$ per donor). The relative luciferase activation (R.L.A) under the treatment of 0.2 μmol/L 9C-RA with concentration-elevated Rald or HX531 in HEK293T cells transfected with the RXR:RXR-DR1 (B), RAR:RXR-DR1 (C) and RAR:RXR-DR5 systems (D) ($n = 3$). Data are mean ± SD. $^{**}P < 0.01$ *vs.* CON group; $^{\#}P < 0.05$, $^{\#\#}P < 0.01$ *vs.* 9C-RA group.

PPARγ did not affect *G6PC* or *PCK1* expression, indicating that the regulation of *PCK1* and *G6PC* by PPARγ is cell-specific. More importantly, Rald attenuated the expression of *PCK1* and *G6PC* mRNA induced by LG100268 but not by TTNPB, demonstrating that Rald may act as an RXR antagonist to downregulate *PCK1* and *G6PC* expression. In contrast, Rald induced *CYP26A* mRNA expression, and this effect was entirely abolished by treatment with the RAR antagonist Ro 41-5253. *CYP26A* is a target gene of RAR[33], and these results further demonstrate that Rald is also an agonist of RAR.

Both RARα and RXRα are abundantly expressed and play essential roles in regulating the expression of their target genes[54]. The luciferase reporter assays results confirmed that Rald is a weak agonist of RARα, with an EC_{50} of 0.53 μmol/L. Both RA and 9C-RA are agonists of RXRα, whose EC_{50} values were 1.44 μmol/L and 47 nmol/L, respectively. These EC_{50} values were significantly higher than the concentrations of RA and 9C-RA reported in human plasma (3.1 nmol/L for RA and 0.1 nmol/L for 9C-RA)[55] and human liver slices (0.1 nmol/g tissue for RA)[56], indicating that RA and 9C-RA have only minor contributions to RXR activation *in vivo*[57]. This is consistent with the results of a previous report[58] showing that OA is an agonist of RXRα, whose EC_{50} (58 μmol/L) value was significantly lower than its concentration in serum (Table S4). Other fatty acids, such as linolenic acid, docosahexaenoic acid, palmitic acid, and stearic acid[57,59], can also bind to and activate RXRα as specific ligands, although with low affinities. These results indicated that RXRα is mainly activated by fatty acids *in vivo*. In contrast, Rald exhibited notable antagonizing effects on RA- or OA-activated RXRα. Molecular docking demonstrated that Rald fit snugly into the RXRα binding pocket but lacked hydrogen bonding with ALA-327, leading to the abduction of helices 11 and 12. The estimated IC_{50} of Rald on the activation of RXRα by OA was 0.18 μmol/L, which was close to the hepatic Rald levels in normal mice and diabetic mice treated with Rald (approximately 0.2−0.3 μmol/L). These results suggest that hepatic Rald deficiency contributes to T2D deterioration by attenuating the inhibitory effects on RXR-mediated PCK1 and G6PC expression, thereby enhancing gluconeogenesis.

RXR recruits other nuclear receptors, such as RAR, PPARγ, farnesoid X-activated receptor, pregnane X receptor, and RXR, for heterodimer or homodimer formation to regulate transcription[5] by binding to different DR regions of target genes[24]. In addition to RXR, PPARγ, and RAR, the importance of farnesoid X-activated receptor and pregnane X receptor in glucose homeostasis has also been gradually discovered, yet no associations with retinoids have been found to date[60−62]. Three binding sites (two DR1 regions and one DR5 region) of RA-related receptors have been identified in the promoter regions of the *PCK1* gene[63], whilst *G6PC* also has two DR1 regions in its promoter[64,65]. Luciferase reporter analysis further confirmed that Rald, serving as an antagonist of RXR, downregulated the expression of *PCK1* and *G6PC* by inhibiting RXR:RXR-DR1 activation, further proving that hepatic Rald deficiency is involved in the deterioration of T2D. Related previous studies have also demonstrated that the RXR antagonist HX531 decreases *PCK1* and *G6PC* expression levels[16], reduces glycemia, and alleviates diabetes[66,67].

Additionally, we found that Rald plus citral treatment increased insulin levels in *db/db* mice (Table S4). Data from INS-1 cells showed that Rald increased cellular insulin synthesis (Supporting Information Fig. S5A−S5D), which may partly explain the increased fasting plasma insulin levels observed in *db/db* mice treated with Rald. However, several reports have demonstrated that fasting serum insulin levels in *db/db* mice are approximately 4−10 times those in normal *db/m* mice[68,69]. *In vivo* experiments showed that even a high dose of insulin could not decrease blood glucose levels in *db/db* mice[70]. Furthermore, we demonstrated that the suppressive effects of insulin on *PCK1* and *G6PC* expression were almost completely abolished in OA-treated HepG2 cells and primary hepatocytes from *db/db* mice (Fig. S5E−S5H). Notably, liver-specific *Raldh1* silencing did not affect fasting plasma insulin levels in *db/db* mice (Table S5) but significantly decreased hepatic PCK1 and G6PC expression and blocked the deterioration of T2D. These results indicate that although Rald increased plasma insulin levels in *db/db* mice, the role of increased insulin levels by Rald in hepatic PCK1 and G6PC expression under T2D conditions were minor and still require further investigation.

5. Conclusions

T2D induces the expression of hepatic RALDH1, leading to a deficiency in hepatic Rald. Rald, serving as an antagonist of RXR, improves glucose homeostasis primarily by inhibiting the RXR/DR1-mediated expression of PCK1 and G6PC. Hepatic Rald deficiency enhances hepatic gluconeogenesis by attenuating the inhibitory effect on the induction of PCK1 and G6PC by RXR activation, which in turn exacerbates the progression of T2D. These results demonstrate the contribution of Rald to T2D progression and highlight the possibility of developing RALDH1 inhibitors or Rald as therapeutic drugs for modulating T2D.

Acknowledgments

This work was supported by the National Natural Science Foundation of China (Nos. 82173884, 82204511, and 82073922), the Jiangsu Funding Program for Excellent Postdoctoral Talent (No. 1412200067, China), and the "Double First-Class" university project (No. CPU2022QZ21, China).

Author contributions

Hanyu Yang: conceptualization, methodology, investigation, data curation, validation, and writing-original draft. Mengxiang Su: methodology, investigation, data curation, and software. Jianjun Zou, Xiaodong Liu, and Li Liu: supervision, conceptualization, writing-review and editing. Ming Liu, Yun Sheng, Liang Zhu, and Lu Yang: investigation, validation, and data curation. Ruijing Mu: investigation and software. All authors reviewed and edited the manuscript and approved the final version.

Conflicts of interest

The authors declare no conflicts of interest.

Appendix A. Supporting information

Supporting data to this article can be found online at https://doi.org/10.1016/j.apsb.2023.06.014.

References

1. Rhee EJ, Plutzky J. Retinoid metabolism and diabetes mellitus. *Diabetes Metab J* 2012;**36**:167−80.
2. Blaner WS. Vitamin A signaling and homeostasis in obesity, diabetes, and metabolic disorders. *Pharmacol Ther* 2019;**197**:153−78.
3. Iqbal S, Naseem I. Role of vitamin A in type 2 diabetes mellitus biology: effects of intervention therapy in a deficient state. *Nutrition* 2015;**31**:901−7.
4. Liu J, Wang Y, Lin L. Small molecules for fat combustion: targeting obesity. *Acta Pharm Sin B* 2019;**9**:220−36.
5. Evans RM, Mangelsdorf DJ. Nuclear receptors, RXR, and the big bang. *Cell* 2014;**157**:255−66.
6. Nallamshetty S, Le PT, Wang H, Issacsohn MJ, Reeder DJ, Rhee EJ, et al. Retinaldehyde dehydrogenase 1 deficiency inhibits PPARγ-mediated bone loss and marrow adiposity. *Bone* 2014;**67**:281−91.
7. Petrosino JM, Longenecker JZ, Ramkumar S, Xu X, Dorn LE, Bratasz A, et al. Paracardial fat remodeling affects systemic metabolism through alcohol dehydrogenase 1. *J Clin Invest* 2021;**131**:e141799.
8. Ziouzenkova O, Orasanu G, Sharlach M, Akiyama TE, Berger JP, Viereck J, et al. Retinaldehyde represses adipogenesis and diet-induced obesity. *Nat Med* 2007;**13**:695−702.
9. Blomhoff R, Rasmussen M, Nilsson A, Norum KR, Berg T, Blaner WS, et al. Hepatic retinol metabolism. Distribution of retinoids, enzymes, and binding proteins in isolated rat liver cells. *J Biol Chem* 1985;**260**:13560−5.
10. Zhai Y, Sperkova Z, Napoli JL. Cellular expression of retinal dehydrogenase types 1 and 2: effects of vitamin A status on testis mRNA. *J Cell Physiol* 2001;**186**:220−32.
11. Blaner WS, Hendriks HF, Brouwer A, de Leeuw AM, Knook DL, Goodman DS. Retinoids, retinoid-binding proteins, and retinyl palmitate hydrolase distributions in different types of rat liver cells. *J Lipid Res* 1985;**26**:1241−51.
12. Krois CR, Vuckovic MG, Huang P, Zaversnik C, Liu CS, Gibson CE, et al. RDH1 suppresses adiposity by promoting brown adipose adaptation to fasting and re-feeding. *Cell Mol Life Sci* 2019;**76**:2425−47.
13. Belyaeva OV, Adams MK, Popov KM, Kedishvili NY. Generation of retinaldehyde for retinoic acid biosynthesis. *Biomolecules* 2019;**10**:5.
14. Molotkov A, Duester G. Genetic evidence that retinaldehyde dehydrogenase Raldh1 (*Aldh1a1*) functions downstream of alcohol dehydrogenase Adh1 in metabolism of retinol to retinoic acid. *J Biol Chem* 2003;**278**:36085−90.
15. Yang D, Vuckovic MG, Smullin CP, Kim M, Lo CP, Devericks E, et al. Modest decreases in endogenous all-*trans*-retinoic acid produced by a mouse Rdh10 heterozygote provoke major abnormalities in adipogenesis and lipid metabolism. *Diabetes* 2018;**67**:662−73.
16. Kiefer FW, Orasanu G, Nallamshetty S, Brown JD, Wang H, Luger P, et al. Retinaldehyde dehydrogenase 1 coordinates hepatic gluconeogenesis and lipid metabolism. *Endocrinology* 2012;**153**:3089−99.
17. Zhang M, Liu C, Hu MY, Zhang J, Xu P, Li F, et al. High-fat diet enhanced retinal dehydrogenase activity, but suppressed retinol dehydrogenase activity in liver of rats. *J Pharmacol Sci* 2015;**127**:430−8.
18. Haenisch M, Treuting PM, Brabb T, Goldstein AS, Berkseth K, Amory JK, et al. Pharmacological inhibition of ALDH1A enzymes suppresses weight gain in a mouse model of diet-induced obesity. *Obes Res Clin Pract* 2018;**12**:93−101.
19. Modak T, Mukhopadhaya A. Effects of citral, a naturally occurring antiadipogenic molecule, on an energy-intense diet model of obesity. *Indian J Pharmacol* 2011;**43**:300−5.
20. Xu D, Wang Z, Xia Y, Shao F, Xia W, Wei Y, et al. The gluconeogenic enzyme PCK1 phosphorylates INSIG1/2 for lipogenesis. *Nature* 2020;**580**:530−5.
21. Hatting M, Tavares CDJ, Sharabi K, Rines AK, Puigserver P. Insulin regulation of gluconeogenesis. *Ann N Y Acad Sci* 2018;**1411**:21−35.
22. Hundal RS, Krssak M, Dufour S, Laurent D, Lebon V, Chandramouli V, et al. Mechanism by which metformin reduces glucose production in type 2 diabetes. *Diabetes* 2000;**49**:2063−9.

23. Zhang R, Wang Y, Li R, Chen G. Transcriptional factors mediating retinoic acid signals in the control of energy metabolism. *Int J Mol Sci* 2015;**16**:14210−44.
24. Mangelsdorf DJ, Evans RM. The RXR heterodimers and orphan receptors. *Cell* 1995;**83**:841−50.
25. Miwa H. High-performance liquid chromatographic determination of mono-, poly- and hydroxycarboxylic acids in foods and beverages as their 2-nitrophenylhydrazides. *J Chromatogr A* 2000;**881**:365−85.
26. Vidyashankar S, Sandeep Varma R, Patki PS. Quercetin ameliorate insulin resistance and up-regulates cellular antioxidants during oleic acid induced hepatic steatosis in HepG2 cells. *Toxicol In Vitro* 2013;**27**:945−53.
27. Zhang DD, Zhang JG, Wu X, Liu Y, Gu SY, Zhu GH, et al. Nuciferine downregulates Per-Arnt-Sim kinase expression during its alleviation of lipogenesis and inflammation on oleic acid-induced hepatic steatosis in HepG2 cells. *Front Pharmacol* 2015;**6**:238.
28. Moreb JS, Mohuczy D, Ostmark B, Zucali JR. RNAi-mediated knockdown of aldehyde dehydrogenase class-1A1 and class-3A1 is specific and reveals that each contributes equally to the resistance against 4-hydroperoxycyclophosphamide. *Cancer Chemother Pharmacol* 2007;**59**:127−36.
29. Liu P, Jiang L, Kong W, Xie Q, Li P, Liu X, et al. PXR activation impairs hepatic glucose metabolism partly *via* inhibiting the HNF4α−GLUT2 pathway. *Acta Pharm Sin B* 2022;**12**:2391−405.
30. Ling Z, Shu N, Xu P, Wang F, Zhong Z, Sun B, et al. Involvement of pregnane X receptor in the impaired glucose utilization induced by atorvastatin in hepatocytes. *Biochem Pharmacol* 2016;**100**:98−111.
31. Hazlehurst JM, Woods C, Marjot T, Cobbold JF, Tomlinson JW. Non-alcoholic fatty liver disease and diabetes. *Metabolism* 2016;**65**:1096−108.
32. Wang L, Liu Q, Kitamoto T, Hou J, Qin J, Accili D. Identification of insulin-responsive transcription factors that regulate glucose production by hepatocytes. *Diabetes* 2019;**68**:1156−67.
33. Loudig O, Babichuk C, White J, Abu-Abed S, Mueller C, Petkovich M. Cytochrome P450RAI (CYP26) promoter: a distinct composite retinoic acid response element underlies the complex regulation of retinoic acid metabolism. *Mol Endocrinol* 2000;**14**:1483−97.
34. Kojetin DJ, Matta-Camacho E, Hughes TS, Srinivasan S, Nwachukwu JC, Cavett V, et al. Structural mechanism for signal transduction in RXR nuclear receptor heterodimers. *Nat Commun* 2015;**6**:8013.
35. Fu J, Si P, Zheng M, Chen L, Shen X, Tang Y, et al. Discovery of new non-steroidal FXR ligands *via* a virtual screening workflow based on phase shape and induced fit docking. *Bioorg Med Chem Lett* 2012;**22**:6848−53.
36. Fernández-Alvarez A, Alvarez MS, Gonzalez R, Cucarella C, Muntané J, Casado M. Human SREBP1c expression in liver is directly regulated by peroxisome proliferator-activated receptor alpha (PPARalpha). *J Biol Chem* 2011;**286**:21466−77.
37. Zhang X, Chen L, Hardwick JP. Promoter activity and regulation of the CYP4F2 leukotriene B_4ω-hydroxylase gene by peroxisomal proliferators and retinoic acid in HepG2 cells. *Arch Biochem Biophys* 2000;**378**:364−76.
38. Durand B, Saunders M, Leroy P, Leid M, Chambon P. All-*trans* and 9-*cis* retinoic acid induction of CRABPII transcription is mediated by RAR−RXR heterodimers bound to DR1 and DR2 repeated motifs. *Cell* 1992;**71**:73−85.
39. Li R, Zhang R, Li Y, Zhu B, Chen W, Zhang Y, et al. A RARE of hepatic Gck promoter interacts with RARα, HNF4α and COUP-TFII that affect retinoic acid- and insulin-induced Gck expression. *J Nutr Biochem* 2014;**25**:964−76.
40. Al Tanoury Z, Piskunov A, Rochette-Egly C. Vitamin A and retinoid signaling: genomic and nongenomic effects. *J Lipid Res* 2013;**54**:1761−75.
41. Loudig O, Maclean GA, Dore NL, Luu L, Petkovich M. Transcriptional co-operativity between distant retinoic acid response elements in regulation of Cyp26A1 inducibility. *Biochem J* 2005;**392**:241−8.
42. Kurokawa R, DiRenzo J, Boehm M, Sugarman J, Gloss B, Rosenfeld MG, et al. Regulation of retinoid signalling by receptor polarity and allosteric control of ligand binding. *Nature* 1994;**371**:528−31.
43. Moore MC, Coate KC, Winnick JJ, An Z, Cherrington AD. Regulation of hepatic glucose uptake and storage *in vivo*. *Adv Nutr* 2012;**3**:286−94.
44. Petersen MC, Vatner DF, Shulman GI. Regulation of hepatic glucose metabolism in health and disease. *Nat Rev Endocrinol* 2017;**13**:572−87.
45. Wang L, Yu J, Zhou Q, Wang X, Mukhanova M, Du W, et al. TOX4, an insulin receptor-independent regulator of hepatic glucose production, is activated in diabetic liver. *Cell Metabol* 2022;**34**:158−170.e5.
46. Luo K, Huang W, Qiao L, Zhang X, Yan D, Ning Z, et al. *Dendrocalamus latiflorus* and its component rutin exhibit glucose-lowering activities by inhibiting hepatic glucose production *via* AKT activation. *Acta Pharm Sin B* 2022;**12**:2239−51.
47. Berry DC, Noy N. All-*trans*-retinoic acid represses obesity and insulin resistance by activating both peroxisome proliferation-activated receptor beta/delta and retinoic acid receptor. *Mol Cell Biol* 2009;**29**:3286−96.
48. Ziouzenkova O, Plutzky J. Retinoid metabolism and nuclear receptor responses: new insights into coordinated regulation of the PPAR−RXR complex. *FEBS Lett* 2008;**582**:32−8.
49. Balmer JE, Blomhoff R. Gene expression regulation by retinoic acid. *J Lipid Res* 2002;**43**:1773−808.
50. Zhang Y, Li R, Chen W, Li Y, Chen G. Retinoids induced Pck1 expression and attenuated insulin-mediated suppression of its expression *via* activation of retinoic acid receptor in primary rat hepatocytes. *Mol Cell Biochem* 2011;**355**:1−8.
51. Tontonoz P, Hu E, Devine J, Beale EG, Spiegelman BM. PPAR gamma 2 regulates adipose expression of the phosphoenolpyruvate carboxykinase gene. *Mol Cell Biol* 1995;**15**:351−7.
52. Glorian M, Duplus E, Beale EG, Scott DK, Granner DK, Forest C. A single element in the phosphoenolpyruvate carboxykinase gene mediates thiazolidinedione action specifically in adipocytes. *Biochimie* 2001;**83**:933−43.
53. Davies GF, Khandelwal RL, Wu L, Juurlink BH, Roesler WJ. Inhibition of phosphoenolpyruvate carboxykinase (*PEPCK*) gene expression by troglitazone: a peroxisome proliferator-activated receptor-gamma (PPARgamma)-independent, antioxidant-related mechanism. *Biochem Pharmacol* 2001;**62**:1071−9.
54. Li B, Cai SY, Boyer JL. The role of the retinoid receptor, RAR/RXR heterodimer, in liver physiology. *Biochim Biophys Acta* 2021;**1867**:166085.
55. Arnold SLM, Amory JK, Walsh TJ, Isoherranen N. A sensitive and specific method for measurement of multiple retinoids in human serum with UHPLC−MS/MS. *J Lipid Res* 2012;**53**:587−98.
56. Czuba LC, Wu X, Huang W, Hollingshead N, Roberto JB, Kenerson HL, et al. Altered vitamin A metabolism in human liver slices corresponds to fibrogenesis. *Clin Transl Sci* 2021;**14**:976−89.
57. Wolf G. Is 9-*cis*-retinoic acid the endogenous ligand for the retinoic acid-X receptor?. *Nutr Rev* 2006;**64**:532−8.
58. Goldstein JT, Dobrzyn A, Clagett-Dame M, Pike JW, DeLuca HF. Isolation and characterization of unsaturated fatty acids as natural ligands for the retinoid-X receptor. *Arch Biochem Biophys* 2003;**420**:185−93.
59. Chaikuad A, Pollinger J, Rühl M, Ni X, Kilu W, Heering J, et al. Comprehensive set of tertiary complex structures and palmitic acid binding provide molecular insights into ligand design for RXR isoforms. *Int J Mol Sci* 2020;**21**:8457.
60. Qiu Y, Shen L, Fu L, Yang J, Cui C, Li T, et al. The glucose-lowering effects of α-glucosidase inhibitor require a bile acid signal in mice. *Diabetologia* 2020;**63**:1002−16.

61. Hassani-Nezhad-Gashti F, Rysä J, Kummu O, Näpänkangas J, Buler M, Karpale M, et al. Activation of nuclear receptor PXR impairs glucose tolerance and dysregulates GLUT2 expression and subcellular localization in liver. *Biochem Pharmacol* 2018;**148**:253−64.
62. Ding L, Yang Q, Zhang E, Wang Y, Sun S, Yang Y, et al. Notoginsenoside Ft1 acts as a TGR5 agonist but FXR antagonist to alleviate high fat diet-induced obesity and insulin resistance in mice. *Acta Pharm Sin B* 2021;**11**:1541−54.
63. Shin DJ, Odom DP, Scribner KB, Ghoshal S, McGrane MM. Retinoid regulation of the phosphoenolpyruvate carboxykinase gene in liver. *Mol Cell Endocrinol* 2002;**195**:39−54.
64. Hirota K, Aoyama H, Fukamizu A. Mutation analysis of HNF-4 binding sites in the human glucose-6-phosphatase promoter. *Int J Mol Med* 2005;**15**:487−90.
65. Chopra AR, Louet JF, Saha P, An J, Demayo F, Xu J, et al. Absence of the SRC-2 coactivator results in a glycogenopathy resembling Von Gierke's disease. *Science* 2008;**322**:1395−9.
66. Nakatsuka A, Wada J, Hida K, Hida A, Eguchi J, Teshigawara S, et al. RXR antagonism induces G0/G1 cell cycle arrest and ameliorates obesity by up-regulating the p53-p21(Cip1) pathway in adipocytes. *J Pathol* 2012;**226**:784−95.
67. Yamauchi T, Waki H, Kamon J, Murakami K, Motojima K, Komeda K, et al. Inhibition of RXR and PPARgamma ameliorates diet-induced obesity and type 2 diabetes. *J Clin Invest* 2001;**108**:1001−13.
68. Nonaka Y, Takeda R, Kano Y, Hoshino D. Short-term calorie restriction maintains plasma insulin concentrations along with a reduction in hepatic insulin-degrading enzyme levels in *db/db* mice. *Nutrients* 2021;**13**:1190.
69. Qiao J, Zhang Z, Ji S, Liu T, Zhang X, Huang Y, et al. A distinct role of STING in regulating glucose homeostasis through insulin sensitivity and insulin secretion. *Proc Natl Acad Sci U S A* 2022;**119**:e2101848119.
70. Cipolletta E, Gambardella J, Fiordelisi A, Del Giudice C, Di Vaia E, Ciccarelli M, et al. Antidiabetic and cardioprotective effects of pharmacological inhibition of GRK2 in *db/db* mice. *Int J Mol Sci* 2019;**20**:1492.